THE JOURNAL OF PHYSICAL CHEMISTRY B

Article

pubs.acs.org/JPCB

Molecular Dynamics Simulations of Yeast F_1-ATPase before and after 16° Rotation of the γ Subunit

Yuko Ito,[†] Takashi Yoshidome,[‡] Nobuyuki Matubayasi,[§,∥] Masahiro Kinoshita,[‡] and Mitsunori Ikeguchi*[,†]

[†]Graduate School of Nanobioscience, Yokohama City University, 1-7-29, Suehiro-cho, Tsurumi-ku, Yokohama, 230-0045 Japan
[‡]Institute of Advanced Energy and [§]Institute for Chemical Research, Kyoto University, Gokasho, Uji, Kyoto, 611-0011, Japan
[∥]CREST, Japan Science and Technology Agency (JST), Kawaguchi, Saitama, 332-0012, Japan

Supporting Information

ABSTRACT: We have recently proposed the "packing exchange mechanism" for F_1-ATPase, wherein the perturbation by a substrate binding/release or an ATP hydrolysis is followed by the reorganization of the asymmetric packing structure of the $\alpha_3\beta_3$ complex, accompanying the γ subunit rotation. As part of a further investigation of this rotational mechanism, we performed all-atom molecular dynamics simulations for yeast F_1-ATPase both before and after a 16° rotation of the γ subunit triggered by a Pi release. We analyzed the structural fluctuations, the subunit interface interactions, and the dynamics of the relative subunit arrangements before and after the rotation. We found that with the Pi release the $\alpha_E\beta_E$ subunit interface becomes looser, which also allosterically makes the $\alpha_{DP}\beta_{DP}$ subunit interface looser. This structural communication between these interfaces takes place through a tightening of the $\alpha_{TP}\beta_{TP}$ subunit interface. The γ subunit interacts less strongly with α_{DP} and β_{DP} and more strongly with α_{TP} and β_{TP}. After the Pi release, the tightly packed interfaces are reorganized from the interfaces around β_{DP} to those around β_{TP}, inducing the 16° rotation. These results, which are consistent with the packing exchange mechanism, allow us to deduce a view of the structural change during the 40° rotation.

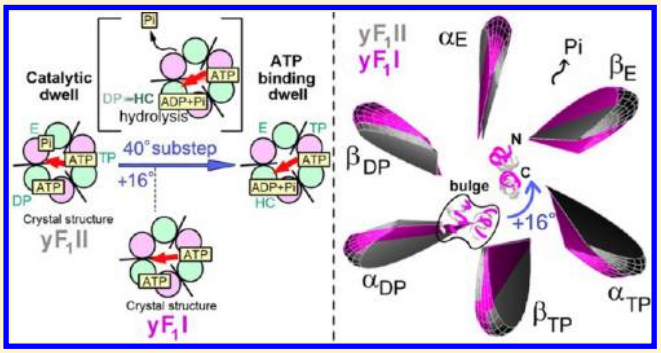

INTRODUCTION

F_1-ATPase is an ATP-driven rotary motor enzyme.[1−11] This enzyme can carry out ATP synthesis/hydrolysis with a reversible motor rotation (Figure 1, inside the rectangular box).[12] ATP synthesis/hydrolysis via a rotation of the γ subunit in F_1-ATPase (the F_1 moiety) is coupled to an electrochemical diffusion gradient across a membrane-embedded unit, F_o.[13] The three-dimensional structure of the F_1-ATPase was determined for the first time in 1994.[14] The $\alpha_3\beta_3$ subunits are arranged hexagonally around the central γ-subunit stalk. Only the β subunit is catalytically active and changes its conformation along with the nucleotide binding/release and ATP hydrolysis. For most crystal structures, the three β subunits are in different states: two closed states (β_{DP} and β_{TP}) and one open state (β_E) (Figure 1). The hydrolysis reaction of F_1-ATPase occurs in the 120° rotation step of the γ subunit,[15] which can be divided further into the 80 and 40° substeps, as described below.[16] The crystal structure corresponds to the structure after the 80° rotation.[17]

A single molecule experiment has revealed the sequential conformational change of the β subunit along with the 120° rotation of the γ subunit (Figure 1).[18] According to the study, before the 80° rotation, the three β subunits in the F_1-ATPase complex take on the closed (β'_{TP}), open (β'_E), and half-closed conformation (β_{HC}) states, respectively, where β_{HC} is the "half-closed" structure and the prime (′) is used to distinguish from the β subunit structures found in the crystal structure. This structure corresponds to the ATP-binding dwell state.[18] Then, the 80° rotation is induced by the ATP binding and the ADP release with the structural change of the two different β subunits, $\beta'_E \rightarrow \beta_{TP}$ and $\beta_{HC} \rightarrow \beta_E$, respectively.[18] After the 80° rotation, the F_1-ATPase complex corresponding to the crystal structure is at the catalytic dwell state.[17] At this state, the ATP hydrolysis occurs for 1 ms.[19] Subsequently, the 40° rotation is induced by the β subunit conformational change, $\beta_{DP} \rightarrow \beta_{HC}$,[18] due to the ATP hydrolysis and the inorganic phosphate (Pi) release from the β_E subunit.[20]

To characterize the rotational mechanism of F_1-ATPase, extensive computer simulations have been performed.[21−34] In our previous study,[33] we conducted a molecular dynamics (MD) simulation for a structure of the catalytic dwell state in bovine F_1-ATPase to determine the structural dynamics properties. It was found that the structure of that state has different fluctuations and interface interactions for each subunit. In particular, the tightly packed interfaces are mostly found around the β_{DP} subunit, while the β_{TP} subunit has relatively weaker interactions at the interfaces, although the β_{TP} subunit is conformationally fairly similar to the β_{DP} subunit and binds

Received: December 19, 2012
Revised: March 1, 2013
Published: March 3, 2013

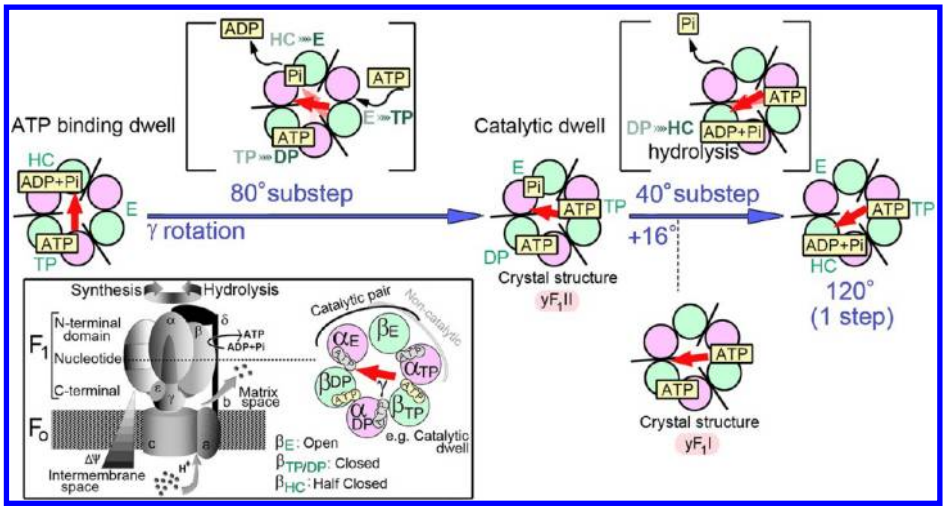

Figure 1. Reaction scheme for the 120° rotation of the γ subunit. The figures inside the brackets indicate each intermediate for the 80 and 40° substeps. The bottom left figure inside the rectangular box indicates the general information for F_1-ATPase: structure of the F_oF_1-ATPase complex and the cross-sectional arrangement of the subunits in the F_1 moiety, viewed from the side of the C-terminal domains.

ATP in the same manner as the β_{DP} subunit. Compared with the other subunits, the β_E subunit has only weakly interacting interfaces with resulting large fluctuations. This asymmetric characteristic of the catalytic dwell state structure suggests that after this state the tightly interacting interfaces around the β_{DP} subunit are loosened due to perturbations such as the ATP hydrolysis and the Pi release, and instead of the β_{DP} subunit interface, the other subunit interfaces reach a tighter packing than in the catalytic dwell state. These subunit rearrangements within the $\alpha_3\beta_3$ complex eventually induce the γ subunit rotation. In addition to the MD simulations, we analyzed the characteristics of the asymmetric packing of the same F_1-ATPase structure in terms of the water-entropy effect using the statistical thermodynamics of molecular liquids.[35] The asymmetric interface interactions observed in the MD simulations were successfully reproduced using a theoretical method focused on the water-entropy effect. We have asserted that this type of asymmetric packing is driven by the water-entropy effect.[35] When the overall, impartial tight packing is not achievable in a protein, the portions that can be tightly packed are chosen for the preferential tight packing to maximize the water entropy in the presence of the F_1-ATPase complex. When a tightly packed portion is perturbed, the structure with the maximum water entropy is recovered by forming a tight packing in the other portion. From these studies, we suggested the following complete (80° + 40°) rotational mechanism: an event (the ATP binding, release of the ADP/Pi, and the ATP hydrolysis) occurs; the asymmetric $\alpha_3\beta_3$ complex structure is perturbed, leading to a decrease in the water entropy; and tightly or weakly interacting interfaces are reorganized within the $\alpha_3\beta_3$ complex ring, letting the γ subunit rotate and resulting in the maximization of the water entropy of the system. We refer to this mechanism as the "packing exchange mechanism". In this mechanism, the complex always tries to form three regions that are tightly packed, moderately packed, and loosely packed, respectively, and these regions are cyclically exchanged.

Additionally, the importance of the packing rearrangement in the $\alpha_3\beta_3$ complex is supported by experiments. In single molecule studies,[36,37] with most of the γ axle truncated, the γ subunit still rotated in the correct direction with the ATP hydrolysis. Even without the γ subunit, the unidirectional β subunit conformational changes in the presence of ATP were observed in an atomic force microscopy (AFM) study.[38] These data clearly indicate that the sequential packing exchange in the $\alpha_3\beta_3$ asymmetric ring is primarily responsible for the γ subunit rotation.

A limitation of our previous studies is that the MD simulation and the study of the statistical thermodynamics of molecular liquids were applied to only the catalytic dwell state structure.[33,35] The information for a single state is not enough to predict the sequential changing structure during the rotational transition, but most of the available crystal structures represent this catalytic dwell state. One of the very few exceptions (crystal structures of yeast F_1-ATPase with a crystallographic unit containing two different states) was reported in 2006.[39] These two structures are referred to as yF_1I and yF_1II. The structure yF_1II corresponds to the catalytic dwell state, with a structure similar to other existing crystal structures. In the other structure, yF_1I, the central stalk is rotated +16° in the hydrolysis direction (Figure 1). Accordingly, these structures are suitable for studying the sequentially changing structures and for characterizing the rotational mechanism. The yF_1II complex binds Pi in the β_E subunit and yF_1I liberates it, making further structural differences between the two; the $\alpha_E\beta_E$ and $\alpha_{DP}\beta_{DP}$ subunit interfaces in yF_1I are more open by 3.7 and 5.5°, respectively, than those in yF_1II.[39] Since single molecule experiments demonstrated that the Pi release occurs at the β_E subunit and the γ subunit is rotated after the ATP hydrolysis and the Pi release,[20,40] these yF_1II and yF_1I structures are supposed to represent snapshots of before and after the Pi release in the 40° substep, respectively. With the adenylyl imidiodiphosphate (AMP-PNP) molecule bound to the β_{DP} catalytic site in those crystal structures, yF_1I corresponds to the structure after the Pi release but before the completion of the ATP hydrolysis.

For both yF_1II and yF_1I, we performed all-atom MD simulations to obtain the structural dynamics information both before and after the Pi release, respectively. The thermal fluctuations observed at equilibrium are a good indicator of the intrinsic flexibility of proteins.[41,42] The differences in the fluctuations between the two states will be reflected in their asymmetric responses upon the rotation. Therefore, from the structural fluctuations of yF_1II and yF_1I, the subunit interface interactions and the dynamics of the relative subunit arrange-

dx.doi.org/10.1021/jp312499u | J. Phys. Chem. B 2013, 117, 3298−3307

ments were investigated. As the Pi release is the main torque generating element for the 40° substep,[20,40] we compared the dynamics data both before and after the 16° rotation, and the results allow us to propose the structural change mechanism of the 40° substep. In this article, we describe how the F_1-ATPase complex changes the structure after the Pi release, based on the results of the MD simulations for yF_1II and yF_1I. Then, we propose a possible mechanism for the 40° rotation of the γ subunit.

MATERIALS AND METHODS

Initial Structures. The yF_1II and yF_1I structures of 2HLD (PDB ID)[39] were used as the initial structures for the MD simulation. The missing residues (yF_1II: α_E407−409, α_{TP}408−410, α_{DP}408 and 409, γ59−70; yF_1I: α_E408 and 409, α_{TP}408 and 409, γ60−70) were modeled using MODELER,[43] based on the 1E79 (PDB ID) crystal structure.[44] To model the γ subunit of yF_1II and yF_1I, the missing part of the γ subunit in yF_1II was first restored. As the root-mean-square deviation (RMSD) of the γ subunit (the Cα atom) between yF_1II and yF_1I is fairly small (1.22 Å), the yF_1II atomic coordinates superimposed onto the γ subunit in yF_1I using FATCAT[45] were used as the γ subunit of yF_1I. These modeled structures were optimized by energy minimization. The AMP-PNP molecules in the subunits except for the β_E subunit of the original crystal structures were replaced by ATP, since the complex structures are supposed to be at the states before and after the Pi release of the catalytic dwell state.[17,20,40] The nucleotide state in each subunit of the simulated yF_1II and yF_1I complexes is summarized in Supporting Information, Table S1.

MD Simulations. The structures were solvated in a box of water. Ion concentrations (Na^+ and Cl^-) were set to ∼150 mM. The total numbers of atoms were 311 633 for yF_1I and 316 224 for yF_1II, including 262 842 (yF_1I) and 267 357 (yF_1II) atoms for the water molecules; 478 (Na^+: 261 and Cl^-: 217, yF_1I) and 487 (Na^+: 266 and Cl^-: 221, yF_1II) atoms for the ions; and 220 (5 × Mg^{2+}-ATP: 5 × 44) and 227 (5 × Mg^{2+}-ATP and $H_2PO_4^-$: 5 × 44 + 7) for the nucleotides. The initial distance between the periodic images of the protein was 28.0 Å. After a minimization of the initial structures for 6000 steepest descent steps, the system was heated from 1 to 300 K with harmonic constraints of 1.0 kcal/mol/Å^2 on the non-hydrogen atoms of the solute under NVT ensemble conditions for 100 ps. Subsequently, the force constant was gradually decreased to 0 over 100 ps under NPT conditions. After this equilibration, sampling simulations were performed under the NPT ensemble conditions for 100 ns. The average box lengths and density during the 100 ns simulations are summarized in Supporting Information, Table S2.

All simulations were performed with the MD program MARBLE,[46] using CHARMM22/CMAP[47,48] for protein and TIP3P[49] for water as the force field parameters. Electrostatic calculations were performed using the particle mesh Ewald (PME) method with a grid spacing of ∼1 Å.[50] The Lennard-Jones potential and the real-space interactions for the PME were truncated at 10 Å. The symplectic integrator for rigid bodies was used for the constraints of the bond lengths and angles involving hydrogen atoms.[46] A time step of 2.0 fs was used.

Contact Analysis and Root-Mean-Square Fluctuation (RMSF). To characterize the structures of yF_1II and yF_1I, their subunit interface interactions and structural fluctuations were determined using a contact analysis[51] and RMSF calculations, respectively. In the contact analysis, residue pairs maintaining their intersubunit interactions within a certain distance over a certain percentage of the MD trajectory were picked up. For this study, basic threshold values less than 4.5 Å for the interatomic distance for more than 98% of the MD trajectory were used. Residue pairs detected by these threshold values indicated that, although those residues reside on different neighboring subunits, they stay close to each other during the entire MD simulation. In other words, the subunit interface around the selected residue pairs was tightly packed. Hereinafter, the contacts between the residue pairs are referred to as "stable contacts". The RMSF is defined as $\mathrm{RMSF}(i) = [\langle(\mathbf{R}_i - \langle\mathbf{R}_i\rangle)^2\rangle]^{1/2}$, where $\mathbf{R}_i$ is the position vector of atom i (in this study, only the Cα atom coordinates were evaluated), and the broken brackets represent the time average over the entire trajectory. The RMSF indicates the intensity of the structural fluctuation for each residue. In our previous study,[33] the subunit interface interactions determined by the contact analysis affected the magnitude of the structural fluctuation (e.g., a tightly packed interface suppresses structural fluctuation, while a loose interface allows the structure to fluctuate widely). The RMSF values were calculated from the last half of the MD trajectory which is the equilibrated state. Also, the simulations do not include the ε subunit or the c subunit ring, so that the protruding region of the γ subunit (Ser40-Thr220) is substantially flexible. For this reason, the fit of the structure relative to a reference (the starting structure) in the RMSF calculation was performed without the protrusion.

C-Terminal Domain. The α and β subunits consist of three domains: the N-terminal, the nucleotide-binding, and the C-terminal domains (Figure 1, inside the rectangular box). In our previous study,[33] distinct differences for the structural fluctuation and the interface configuration for the α and β subunits were observed in the C-terminal domain. In the F_1-ATPase complex, the three β subunits with different nucleotide binding states create the asymmetric hexameric structure. Depending on the nucleotide state, the most distinct structural differences in the β subunit are found in the C-terminal domain. Hence, the structural investigations of yF_1II and yF_1I using the contact analysis and the RMSF calculations were primarily focused on the C-terminal domain.

RESULTS AND DISCUSSION

Structural Fluctuations and Stable Contacts in yF_1II and yF_1I. The RMSF calculation and the contact analysis were applied to yF_1II and yF_1I. The RMSF data are shown in Figure 2A−D. The magnitudes for the C-terminal domain are summarized in Figure 2E,F. In the same figure, the total numbers of stable contacts between the neighboring subunits are also shown (the result details for the stable contacts are presented in Supporting Information, Figures S1 and S2). The data clearly show that the fluctuation tendency and the interface configuration for each subunit are different between yF_1II and yF_1I.

In the C-terminal domain of yF_1II, the order of the magnitude for the structural fluctuation is $\beta_{DP} < \beta_{TP} < \beta_E$ (Figure 2C), which is the same as the order of the catalytic dwell state structure in the bovine F_1-ATPase determined in a previous MD simulation.[33] This order of the RMSF magnitude is interpreted using the subunit interface interactions derived from the contact analysis. Figure 2E shows that the β_{DP} subunit has stable contacts in all β_{DP} subunit interfaces (both sides of the α subunits and the γ subunit), indicating that the β_{DP}

dx.doi.org/10.1021/jp312499u | J. Phys. Chem. B 2013, 117, 3298−3307

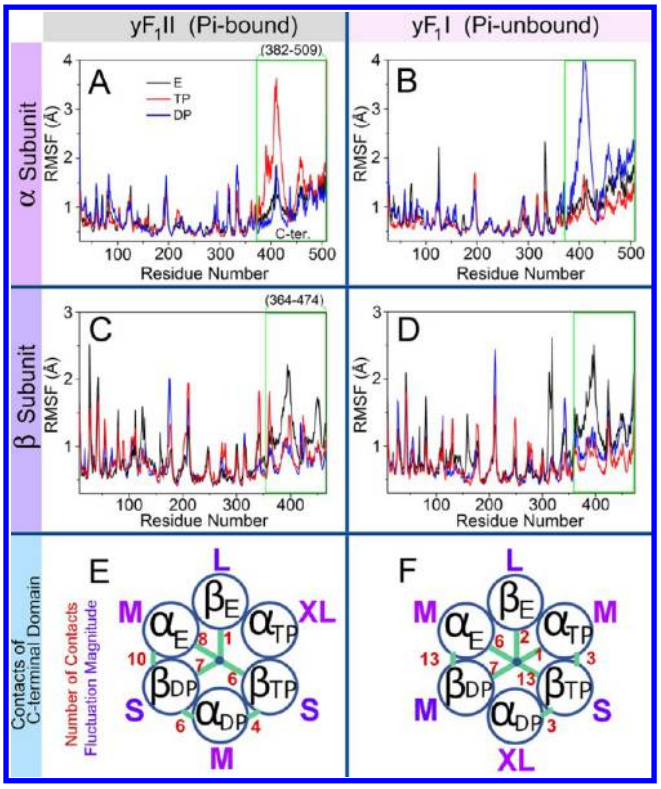

Figure 2. RMSF as a function of the residue number for the α subunits in (A) yF_1II and (B) yF_1I, and for the β subunits in (C) yF_1II and (D) yF_1I. Parts enclosed by green rectangles indicate the C-terminal domain. Summary of the fluctuation magnitude and the number of the interface contacts for the C-terminal domain in (E) yF_1II and (F) yF_1I. "S", "M", "L", and "XL" indicate small, medium, large, and extra large, respectively, for the RMSF of three α or β subunits, which is defined by the average of the RMSF value in the C-terminal domain; "S" means that the value is below 1.0 Å; "M", the value is between 1.0 and 1.3 Å; "L", the value is between 1.3 and 1.5 Å; and "XL", the value is over 1.5 Å. The numbers outside and inside the F_1 complex model indicate the net number of stable contacts in the interface of the C-terminal domain between the α and β subunits as well as between the α/β and γ subunits, respectively. Further data on the stable contacts are presented in Supporting Information, Figures S1 and S2.

subunit interacts intensively with all neighboring subunits. As these tight interface interactions restrict fluctuations, the fluctuation magnitude of the β_{DP} subunit is the smallest among the three β subunits. The β_{TP} subunit has stable contacts with only one α subunit (α_{DP}) and the γ subunit. For the β_E subunit, the stable contacts are scarce. Consequently, the magnitudes of the fluctuation of the C-terminal domain for the β_{TP} and β_E subunits are larger than in the β_{DP} subunit. Despite the similar conformations between the closed β_{DP} and β_{TP} subunits (the Cα RMSD between the two is 0.55 Å in the yF_1II crystal structure), the β_{DP} subunit exhibits smaller fluctuations than the β_{TP} subunit due to dissimilar interface interactions. For yF_1II, only the α_{TP} subunit does not have any stable contacts with all neighboring subunits, allowing substantial fluctuations (Figure 2A,E). These interface interactions in yF_1II are also similar to the interactions determined for the bovine F_1-ATPase structure.[33]

For yF_1I, the order of the magnitude for the structural fluctuation of the C-terminal domain is $\beta_{TP} < \beta_{DP} < \beta_E$ (Figure 2D). This fluctuation order, which is different from that determined for yF_1II, can also be explained by subunit interface interactions. The β_{TP} subunit, which does not have any stable contacts with the α_{TP} subunit in yF_1II, gains the contacts in yF_1I (Figure 2E,F). These gained contacts are depicted as a contiguous surface in Figure 3, appearing as red marks in the C-terminal domain in those subunits (Figure 3, panel 3). Contrary to the β_{TP} subunit, the β_{DP} subunit, whose fluctuation is not the smallest in yF_1I, loses contacts with neighboring subunits (Figure 2E,F). In particular, the stable contacts found in the C-terminal domain of the $\alpha_{DP}\beta_{DP}$ subunit interface for yF_1II are completely absent in Figure 3 (panel 5).

In summary, both before and after the Pi release, the subunit interface rearrangements occur in the $\alpha_3\beta_3$ complex, inverting the order of the fluctuation magnitude for each subunit. Before the Pi release, the β_{DP} subunit has the smallest fluctuations due to the strong interactions with all neighboring subunits. When the Pi release occurs, these tight interactions become weakened, intensifying the interactions at the interface between the β_{TP} subunit and the neighboring subunits. Therefore, the smallest magnitude of the fluctuation is found in the β_{TP} subunit. The rearrangement of the tight packing at the $\alpha_{DP}\beta_{DP}$ to $\alpha_{TP}\beta_{TP}$ subunit interface is consistent with our recent analysis,[52] examining yF_1II and yF_1I using statistical thermodynamics of molecular liquids. These subunit interface rearrangements support the packing exchange mechanism.[33,35] Additionally, interestingly, the Pi release at the $\alpha_E\beta_E$ subunit interface appears to reduce the interactions at the $\alpha_{DP}\beta_{DP}$ subunit interface, where the ATP hydrolysis is supposed to take place. These

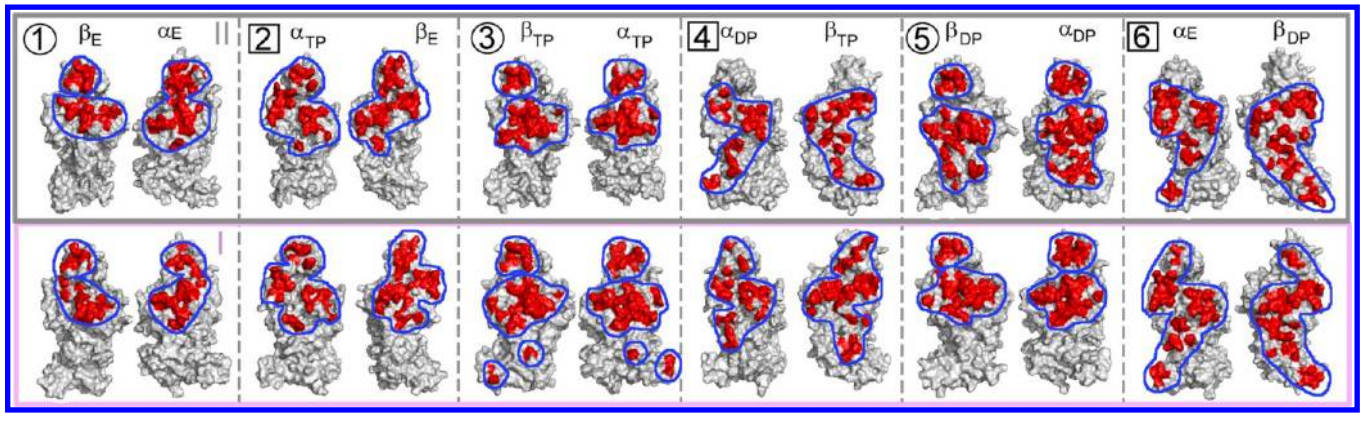

Figure 3. Stable contacts (in red) that maintain the interatomic distance at less than 4.5 Å for more than 98% of the MD trajectories. The panel numbers (1–6) are matched to Figure 6B. The top and bottom panels indicate yF_1II and yF_1I, respectively.

dx.doi.org/10.1021/jp312499u | J. Phys. Chem. B 2013, 117, 3298–3307

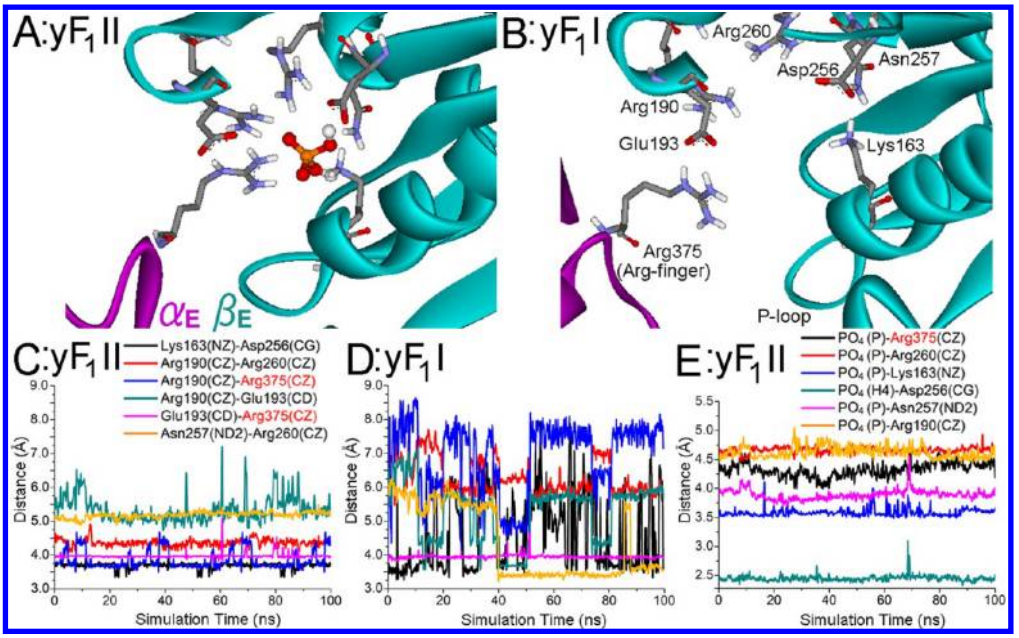

Figure 4. MD snapshots for the Pi binding site in the $\alpha_E\beta_E$ subunit interface in (A) yF_1II and (B) yF_1I. Plots of the distances between pairs of Pi binding residues during the MD simulation of yF_1II and yF_1I are shown in (C) and (D), respectively. The line color coding in (D) is the same as in (C). Distances between Pi and the binding residues during the yF_1II MD simulation are plotted in (E). Arg375 (red) is recognized as an "arginine finger", which is drawn from the α subunit and in charge of the ATP binding and hydrolysis (C and E).

differences between yF_1II and yF_1I are assumed to have originated from the phosphate binding state in the β_E subunit. In the following sections, three topics are covered: the differences of the $\alpha_E\beta_E$ subunit interface associated directly with the Pi release, several distinctive structural features in the overall $\alpha_3\beta_3$ complexes originating from the differences of the $\alpha_E\beta_E$ subunit interface, and the interface interactions between the $\alpha_3\beta_3$ complex and the γ subunit for yF_1II and yF_1I.

Comparison of the $\alpha_E\beta_E$ Subunit Interfaces between yF_1II and yF_1I. We investigated the effects of Pi binding/unbinding on the local structure of the phosphate binding site in the $\alpha_E\beta_E$ subunit interface. An analysis of these effects on the entire $\alpha_E\beta_E$ interface was also performed.

The behaviors of the phosphate binding sites in the MD trajectories of yF_1II and yF_1I were investigated by monitoring the distances between the phosphate binding residues. For yF_1II, the distances between each residue remain stable (Figure 4C). The distances between the phosphate and the binding residues also remain constant (Figure 4E). These results indicate that the structure of the phosphate binding site in yF_1II is rigid and fairly stable. In contrast, the distances between the phosphate binding residues in yF_1I change substantially during the MD simulation (Figure 4D). Compared with the yF_1II results, most distances in yF_1I are elongated, indicating that the phosphate binding site is expanded. After the Pi release, the binding pocket formed by the α_E and β_E subunits becomes looser and more flexible. Under physiological conditions, when Pi is released into the surrounding solvent, the released Pi and its binding pocket are stabilized by water molecules and ions,[53,54] indicating that the Pi release occurs spontaneously. However, since the time constant for the Pi release is submilliseconds,[20,40] our simulation time is too short to observe the Pi release from the yF_1II structure.

To examine the effects of this loosened Pi binding site on the entire position of the β_E subunit relative to the α_E subunit, we conducted a contact analysis on this $\alpha_E\beta_E$ subunit interface for yF_1II and yF_1I. As shown in Figure 3 (panel 1), the results for yF_1II and yF_1I are similar using the following threshold conditions: less than a 4.5 Å interatomic distance with contacts being maintained for more than 98% of the MD trajectory, indicating permanent interactions. With a gradual reduction in the latter threshold value from 98 to 70% (a point where the residue pairs interact with each other with moderate frequency), different results characterizing the $\alpha_E\beta_E$ subunit interface for each structure appear. Examining these contacts, the residue pairs found only in yF_1II (i.e., after the Pi release these residue combinations no longer interact even with a moderate frequency) are distinguished by the pink color (Figure 5). The pink lines are found in the interfaces of all domains (the N-terminal, nucleotide, and C-terminal domains). Viewed from the C-terminal domain (in Figure 5, bottom), the pink lines appear mainly in the side facing the γ subunit. From both the top and the bottom figures in Figure 5, the overall $\alpha_E\beta_E$ subunit interface in yF_1II, particularly the side facing the γ subunit, loses the contacts, suggesting that after the Pi release that part of the interface becomes looser and more flexible.

These results indicate that after the Pi release the substantially fluctuating Pi binding residues make the global $\alpha_E\beta_E$ subunit interface looser and more flexible. This finding is consistent with a study by Okazaki et al.[55] In an analysis of 29 existing crystal structures by principal component analysis (PCA) to characterize the Pi binding to the β_E subunit, they report a positive correlation of the Pi binding with the tightness of the $\alpha_E\beta_E$ subunit interface at both the local and global levels.

Subunit Displacements of the $\alpha_3\beta_3$ Complex after the Pi Release. We investigated the allosteric effect of the loosened $\alpha_E\beta_E$ subunit interface resulting from the Pi release on the entire $\alpha_3\beta_3$ ring structure; the $\alpha_{DP}\beta_{DP}$ and $\alpha_{TP}\beta_{TP}$ interface interactions became weaker and tighter, respectively (Figures 2 and 3). The dynamics of the relative subunit arrangements of the $\alpha_3\beta_3$ complex are analyzed. First, their dynamics are examined using the domain centroids. During the

dx.doi.org/10.1021/jp312499u | J. Phys. Chem. B 2013, 117, 3298−3307

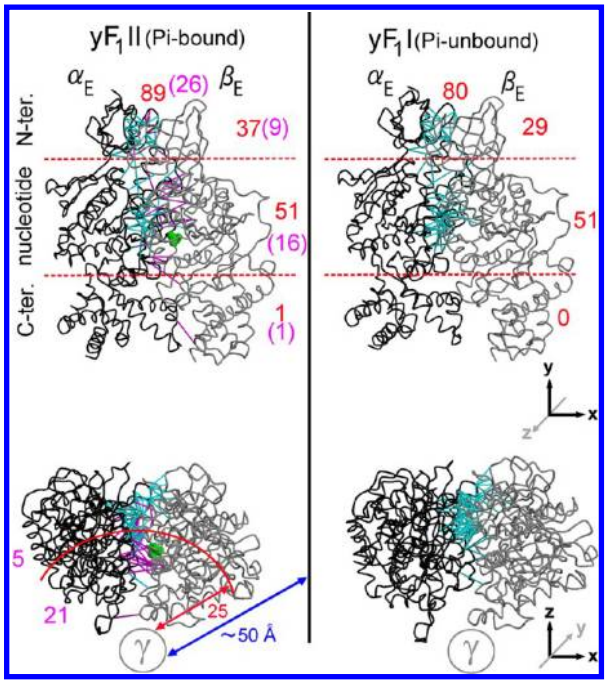

Figure 5. Contact analysis results for the $\alpha_E\beta_E$ interface. Colored lines indicate stable contacts that maintain the interatomic distances at less than 4.5 Å for more than 70% of the MD trajectory. The red numbers written on the left and top indicate the net number of stable contacts in the interface of each domain and the entire structure, respectively. The pink numbers in yF_1II indicate the stable contacts found only in yF_1II. Structures shown at the bottom are obtained by rotating the structures shown above. In the bottom figure for yF_1II, to emphasize the localization of the pink lines, the $\alpha_E\beta_E$ interface is divided into the γ subunit side and the outside interfaces, using a half radius of 25 Å (from the γ subunit to the edge of the α/β subunit is ~50 Å). The pink lines in each section are counted.

entire 100 ns MD simulation, the centroids of domain distances between neighboring subunits are monitored (Figure S3 in the Supporting Information). In particular, distinct distance differences between yF_1II and yF_1I are found in the data of the C-terminal domain. The distances for the last half of the MD trajectories are fairly constant, and to examine the stable part of the trajectories, the last halves of the centroid distances are averaged. Figure 6A shows the average centroid displacements for the three domains (the N-terminal, nucleotide, and C-terminal domains). Centroid distance changes for each subunit interface provide insight into the coupling mechanism for these remotely located subunit interfaces. As previously shown in Figures 2 and 5, the $\alpha_E\beta_E$ subunit interface is loosened with the C-terminal distance stretched by 4.61 Å. At the location for the ATP hydrolysis, the distance of the $\alpha_{DP}\beta_{DP}$ subunit interface is elongated by 4.49 Å. In characterizing this allosteric coupling, we found that the distance is unchanged for the $\alpha_E\beta_{DP}$ subunit pair (indicated by "6" in Figure 6B) that is located on the counterclockwise side (viewed from the C-terminal domain) from the $\alpha_E\beta_E$ subunit pair. For other pairs on the clockwise side, the distances for the $\alpha_{TP}\beta_E$, $\alpha_{TP}\beta_{TP}$, and $\alpha_{DP}\beta_{TP}$ subunit pairs (indicated by "2", "3", and "4" in Figure 6B) are significantly altered (Figure 6A). The largest positional shift in the C-terminal domain is observed for the $\alpha_{TP}\beta_{TP}$ interface with this distance shortened by 6.85 Å. The analysis of these distance changes suggests that the change in the $\alpha_E\beta_E$ interface causes the $\alpha_{DP}\beta_{DP}$ interface to loosen via displacements of the three α_{TP}, β_{TP}, and α_{DP} subunits, rather than that of the single β_{DP} subunit.

To examine the subunit tilting and rotating angles due to the Pi release, the geometric arrangements of the average domain centroids of the $\alpha_3\beta_3$ subunits are described by a three-dimensional model using cut-orange-like objects (Figure 6B). As the Pi release does not induce any intrinsic (open/closed) conformational changes of the β subunit, both the α and the β subunits are simplified to be rigid bodies. This simplification is allowed by the RMSD data (Supporting Information, Table 3) which shows the fairly small values between yF_1II and yF_1I for each subunit. This simplified three-dimensional model accurately describes the actual structure displacements of the C-terminal domain using the tube model (Figure 6C).

The three-dimensional model can be used to visualize the coupling mechanism for the $\alpha_E\beta_E$ subunit interface change with the α_{DP} and β_{DP} subunit displacements via the long ($\alpha_{TP}\beta_{TP}$)

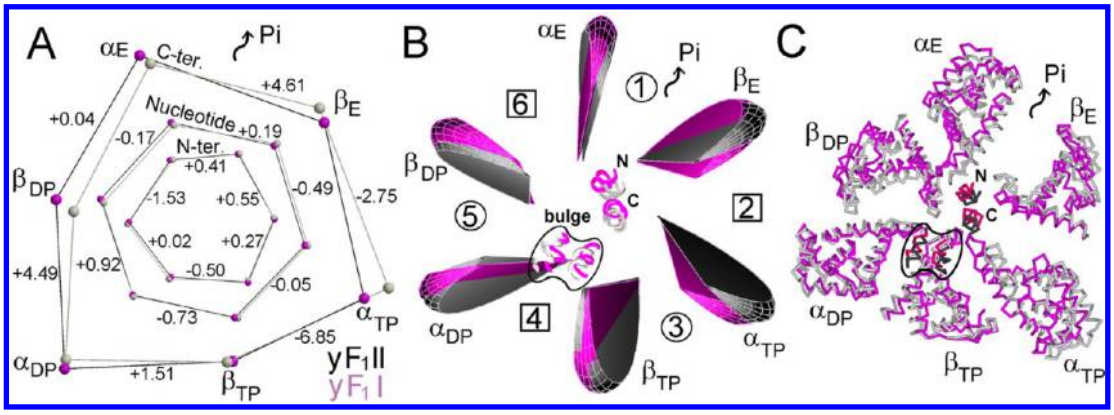

Figure 6. Displacements of the $\alpha_3\beta_3$ complex before (gray) and after (magenta) Pi release as viewed from the C-terminal domain side, where the fit is performed over the N-terminal domain of all the subunits. The centers of mass of the N-terminal, nucleotide, and C-terminal domain for each subunit are shown as spheres, using an average structure of the last half MD simulation (A). The numbers indicate distance changes after the Pi release. Units are in angstroms. The geometric arrangements of the $\alpha_3\beta_3$ subunits are described by a three-dimensional model using cut-orange-like objects (B), with a more detailed explanation described in the text. "N" and "C" indicate the N- and C-terminal α helices of the γ subunit, respectively. The portions for these two α helices are the same as Figure 7 (N, Lys18-Ile25; C, Ala236-Asn243). To indicate the bulge position of the γ subunit, two α helices (residues from Leu91 to His98 and from Lys113 to Arg120) are also presented. The displacements of the C-terminal domain in the last structures of the MD simulations are illustrated by the tube model (C).

dx.doi.org/10.1021/jp312499u | J. Phys. Chem. B 2013, 117, 3298−3307

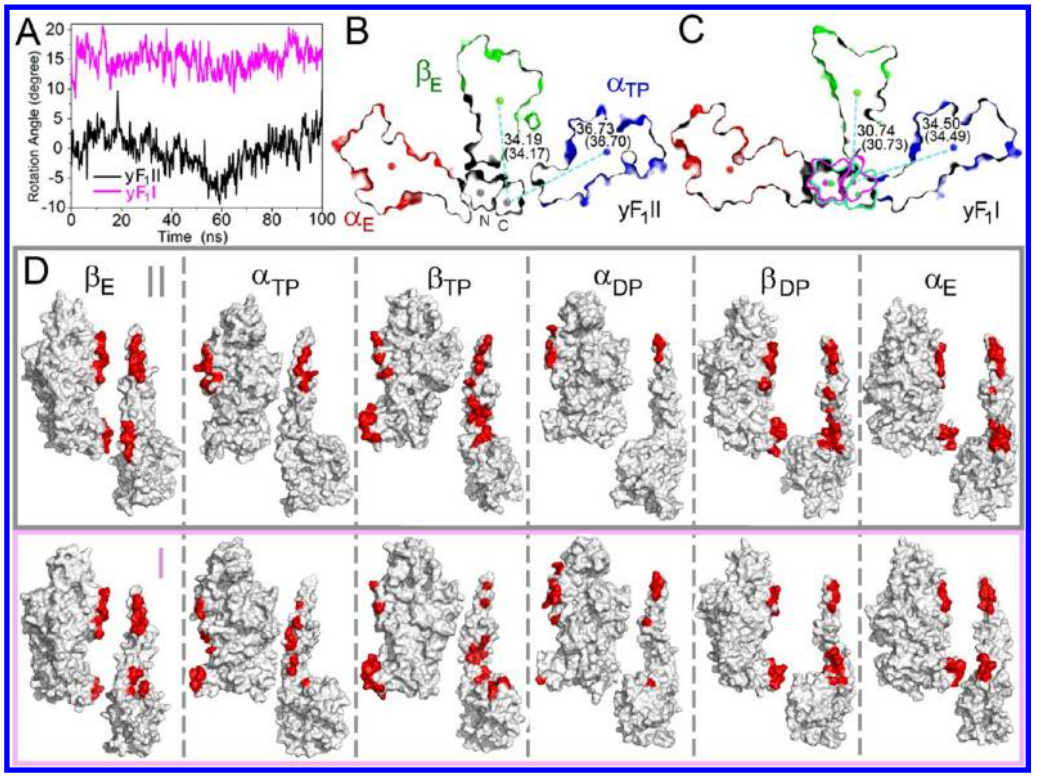

Figure 7. (A) Angles of the γ axis for the 100 ns MD simulations. The portion Lys18-Ile25 is used for the rotational measurement in the article of the original crystal structures.[39] The yF_1II (B) and yF_1I (C) structures are sliced horizontally at the position of residue Asn239 of the γ subunit, where the last structures of the MD simulations are used. The structures are viewed from the side of the C-terminal domain of the α and β subunits. N and C indicate the N- and C-terminal α helices (*N*- and *C*-helices) of the γ subunit. The numbers indicate the distance between the centroids. Units are in angstroms. The numbers inside the parentheses are the same distances in the average structures of the last half of the trajectory. The centroids of the α and β subunits are calculated with the Cα atom of the residues in the C-terminal domain. The centroids of the *N*- and *C*- helices of the γ subunit are calculated with the Cα atoms of the residues from Lys18 to Ile25, and from Ala236 to Asn243, respectively. In (C), the axis of yF_1II (green) is superimposed onto the yF_1I structure (magenta). The fit was performed over the α_E and β_E subunits. Red indicates the stable contacts between the γ and α/β subunits that maintain the interatomic distance at less than 4.5 Å for more than 70% of the MD trajectories (D), where the low-threshold value for the contacts maintaining the percentage of the MD trajectory is used to obtain the difference between yF_1II and yF_1I.

route. Figure 6B indicates that the large distance reduction of the C-terminal domain between the α_{TP} and β_{TP} subunits (Figure 6A) is derived from the tilting α_{TP} subunit. With the Pi release loosening the $\alpha_E\beta_E$ subunit interface, this displacement seems to affect the positional arrangement of the neighboring α_{TP} subunit rather than the β_{DP} subunit. Fluctuating substantially without stable contacts before the Pi release (Figure 2A,E), the α_{TP} subunit has a potential space to accept the displacement. Then, accepting the displacements of the $\alpha_E\beta_E$ subunit interface, the C-terminal domain of the α_{TP} subunit tilts largely toward the β_{TP} subunit. The entire β_{TP} subunit is also withdrawn slightly toward the tilting α_{TP} subunit. With these displacements of the α_{TP} and β_{TP} subunits, the C-terminal domain of the α_{DP} subunit simultaneously tilts toward the β_{TP} subunit side, filling the empty space left by the β_{TP} subunit movement. With the α_{DP} subunit moving away from the β_{DP} subunit, the $\alpha_{DP}\beta_{DP}$ subunit interface becomes loose.

For the $\alpha_3\beta_3$ complex, the subunit displacement results described in this section are consistent with the proposed rotational mechanism of F_1-ATPase. After the 40° rotation, ATP binds to the $\alpha_E\beta_E$ subunit interface[15] and ADP is released from the $\alpha_{DP}\beta_{DP}$ subunit interface,[20] suggesting that these two interfaces should be more open, as indicated by our analysis. For the further 80° rotation (in total, 120°), the current $\alpha_{TP}\beta_{TP}$ subunit interface becomes catalytically active,[56] meaning that the $\alpha_{TP}\beta_{TP}$ subunit interface becomes tighter, which is also consistent with our results.

ATP Binding Site of the $\alpha_{DP}\beta_{DP}$ Subunit Interface. Although the $\alpha_{DP}\beta_{DP}$ subunit interface becomes looser after the Pi release, the structural conformation of the ATP-binding site, including the arginine finger Arg375 (the description of this residue is in the caption of Figure 4) in the $\alpha_{DP}\beta_{DP}$ subunit interface, is fairly similar between yF_1II and yF_1I, as analyzed by measuring the residue distances (Figure S4 in the Supporting Information) and the RMSD value (the heavy atoms RMSD in the ATP-binding site between yF_1II and yF_1I is 0.97 Å). It could be because the β_{DP} subunits in the both yF_1II and yF_1I structures of the MD simulations bind unhydrolyzed ATP, replacing with AMP-PNP in the original crystal structure.[39] This indicates that the Pi release facilitates the loosening of the $\alpha_{DP}\beta_{DP}$ subunit interface, but not beyond changing the ATP-binding site. In fact, a study of the hybrid quantum mechanical/molecular mechanical (QM/MM) methodology[23] verified that the rate-determining step of the ATP hydrolysis in the β_{DP} subunit is a proton transfer from a lytic water molecule, indicating that the ATP hydrolysis mainly involves the local structure around the phosphate group of ATP. According to the results from both the current MD and the QM/MM studies, although the Pi release allosterically makes the $\alpha_{DP}\beta_{DP}$ subunit interface loose, unless the ATP hydrolysis occurs, the local structure around the ATP-binding site is not perturbed,

dx.doi.org/10.1021/jp312499u | J. Phys. Chem. B 2013, 117, 3298−3307

and therefore the conformational change of the β_{DP} subunit ($\beta_{DP} \rightarrow \beta_{HC}$) does not occur. This insusceptibility of the ATP-binding site during the 16° rotation and only local structural involvement for the ATP hydrolysis reflect the weak dependence of the ATP hydrolysis on the angle of the γ subunit rotation.[57]

Position of the γ Subunit. To characterize an induction of the 16° rotation of the γ subunit via the subunit rearrangements of the $\alpha_3\beta_3$ complex due to the Pi release, the positions of the γ subunit relative to the different $\alpha_3\beta_3$ complexes in yF_1II and yF_1I were investigated. As shown in Figure 7A, the two γ subunits maintain their positions (the γ axis of yF_1I is rotated 16° to the hydrolysis direction from the yF_1II) during the entire MD simulations. In the results of the contact analysis with the γ subunit, there are distinctive differences between yF_1II and yF_1I. After the Pi release, the α_{TP} and β_{TP} subunits gain stable contacts with the γ subunit (Figure 2E,F). According to the contiguous surface figures (Figure 7D), the additional α_{TP} and β_{TP} contacts with the γ subunit appear in the C-terminal domain of both the α_{TP} and β_{TP} subunits, appearing on the γ subunit side in the coiled coil helices and the bulge moiety, respectively. Gaining contacts with the γ subunit in the α_{TP} and β_{TP} subunits are also found in the calculated contacted surface areas in the average structures of the MD trajectory (Figure S5 in the Supporting Information). The contacted surface area in the β_{DP} subunit with the γ subunit is reduced in this data, although its distinctive differences are not found in the results of the contact analysis. These observations, that the α_{TP} and β_{TP} subunits gain contacts not only in the $\alpha_3\beta_3$ subunit complex but also with the γ subunit, suggest that after the Pi release the tightly packed interface regions are reorganized from the interfaces around the β_{DP} to those around the β_{TP} subunit, supporting the proposed rotational mechanism.[33,35]

Also, we analyzed the relative position of the γ subunit to the $\alpha_E\beta_E$ subunit interface that is directly involved in the Pi release. After the Pi release, our analysis suggested that this interface becomes looser and more flexible. The results of the contact analysis (Figure 7D) suggest that after the Pi release the contacting regions of the γ subunit with the β_E subunit are shifted. This shift is not observed with the α_E subunit. To obtain a concrete relative position of the γ rotor to the $\alpha_E\beta_E$ subunits, a cross section of the C-terminal domain in these subunits (Figure 7B,C) is examined (the selected portion for the centroid of the γ axis is described in the caption of Figure 7). When the fit is performed over the α_E and β_E subunits, the γ rotor appears to be rotating around the center of the N-terminal α helix (the *N*-helix) of the γ subunit. Therefore, the apparent distance and interface between the α_E subunit and the *N*-helix of the γ subunit in the contiguous surface are hardly changed (Figure 7C,D). In contrast, the distance between the β_E and γ subunits, whose contacting surface regions are shifted, is shortened by 3.5 Å (the measurement detail of the centroid distance is described in Figure 7). These data indicate that the γ rotor leans into the loosened $\alpha_E\beta_E$ interface, centering around the *N*-helix of the γ axis (Figure 7C). With the leaning of the γ subunit, the distance between the neighboring α_{TP} subunit and the C-terminal α helix of the γ subunit is shortened by 2.2 Å, which is related to the results demonstrating that the α_{TP} subunits gain the contacts in the helix region (described above). This axis leaning is the 16° rotation of the γ axis. The results imply that the γ subunit rotation appears to be coupled with the loosening $\alpha_E\beta_E$ subunit interface. These results are supported by a crystal structure study using PCA,[55] determining that the loose/tight motion of the $\alpha_E\beta_E$ subunit interface is tightly correlated with the γ rotational motion. Our results are also consistent with the strong dependence of the Pi release on the angle of the γ subunit rotation.[40]

Summary of the Mechanism for the 16° Rotation of the γ Subunit. The results of the entire subunit rearrangements are summarized in this section (Figure 8). With the Pi release, the $\alpha_E\beta_E$ subunit interface becomes looser and more flexible, allosterically causing the $\alpha_{DP}\beta_{DP}$ subunit interface to loosen as well. This structural communication between these two interfaces takes place through a tightening of the $\alpha_{TP}\beta_{TP}$ subunit interface. Interactions between the γ subunit with the α_{DP} and β_{DP} subunits weaken, as the interactions with the α_{TP} and β_{TP} subunits strengthen. With the displacement of the γ subunit, the γ axis leans into the loosened $\alpha_E\beta_E$ subunit interfaces. After the Pi release, the tightly packed interfaces are reorganized from the interfaces around the β_{DP} to those around the β_{TP} subunit, inducing the 16° rotation. This view for the 16° rotation is consistent with the results suggested from an analysis of the water-entropy effect.[52] We note that the thermodynamic properties were previously analyzed (in ref 52), while the structural dynamics are the focus of the present study. These analyses are closely related. With the formation of a tightly packed interface by the water-entropy effect, the structural fluctuations at the interface are highly suppressed.

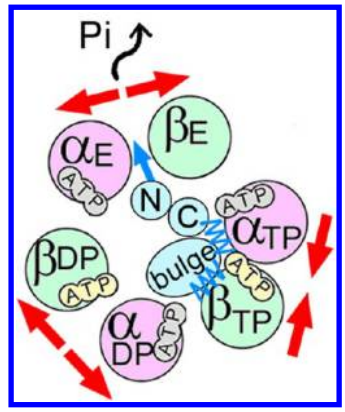

Figure 8. Summary of the subunit rearrangements after the Pi release. Cyan color indicates the γ subunit. "N" and "C" indicate the N- and C-terminal α helices of the γ subunit.

Proposed Mechanism for the Structural Change in the 40° Substep. The current simulation results exhibit the structural displacement after the 16° rotation of the γ subunit, which corresponds to the state after the Pi release, but before the ATP hydrolysis. In fact, the 40° rotation of the γ subunit is induced by both the ATP hydrolysis and the Pi release. The effect of the Pi release can be isolated in the systems simulated in the present study. On the basis of the present results combined with past theoretical and experimental insights, we deduce a view of the structural changes occurring during the 40° rotation of F_1-ATPase.

The ATP hydrolysis depends weakly on the angle of the γ subunit.[57] Our simulation results are consistent with this weak dependence. The local structures of the ATP-binding site remain similar before and after the 16° rotation of the γ subunit (Figure S4 in the Supporting Information), suggesting that the local structures of the ATP-binding site are insusceptible to the rotation angle of the γ subunit in the range of ~10°. In contrast, the Pi release is strongly dependent on the angle of the γ

dx.doi.org/10.1021/jp312499u | J. Phys. Chem. B 2013, 117, 3298−3307

subunit.[20,40] Our simulation results are also consistent with the strong angle dependence. With the Pi release, the $\alpha_E\beta_E$ interface becomes looser at both the local and global levels, contributing to the γ subunit rotation. The loosening of the $\alpha_E\beta_E$ subunit interface allosterically makes the $\alpha_{DP}\beta_{DP}$ subunit interface looser through a tightening of the $\alpha_{TP}\beta_{TP}$ subunit interface and the γ subunit. Once the tightly packed $\alpha_{DP}\beta_{DP}$ subunit interface is allosterically perturbed, both the loosened interfaces and the ATP hydrolysis concertedly allow conformational changes in the β_{DP} subunit from the closed to half-closed form ($\beta_{DP} \rightarrow \beta_{HC}$).[18] These conformational changes of the $\alpha_3\beta_3$ complex drive the 40° rotation. Consequently, it is not until both the Pi release and the ATP hydrolysis are accomplished that the F_1-ATPase completes the 40° rotation of the γ subunit.

The results of the two individual equilibrium MD simulations before and after the 16° rotation contribute to this proposal for the 40° substep mechanism. The structural dynamics in the two different states are informative for elucidating the rotational mechanism. To complement the mechanism thus proposed, advanced simulation techniques investigating the dynamical process of interconversion between the states are currently in progress.

■ ASSOCIATED CONTENT

Supporting Information

Complete ref 47. Contacted analysis results (Figures S1 and S2); monitored distances of subunits for 100 ns MD simulations (Figure S3); snapshots of the structure around the ATP-binding site in the β_{DP} subunit for yF_1II and yF_1I (Figure S4); information of contacted area for each subunit interface in yF_1II and yF_1I (Figure S5); nucleotide state in each subunit of the yF_1II and yF_1I complex for the simulations (Table S1); average box lengths and density during the sampling simulations (Table S2); RMSD values for each subunit between the yF_1II and yF_1I structures (Table S3). This material is available free of charge via the Internet at http://pubs.acs.org.

■ AUTHOR INFORMATION

Corresponding Author

*Tel.: +81-45-508-7232. Fax: +81-45-508-7367. E-mail: ike@tsurumi.yokohama-cu.ac.jp.

Notes

The authors declare no competing financial interest.

■ ACKNOWLEDGMENTS

The authors acknowledge the useful discussion on this work with Dr. Hiroshi Ueno, Department of Physics Faculty of Science and Engineering, Chuo University. This work was supported by a Grant-in-Aid for the Japan Society for the Promotion of Science (JSPS) fellows (24.7915); by Grants-in-Aid for Scientific Research on Innovative Areas (Grants 20118002, 20118004, and 21118519) from the Ministry of Education, Culture, Sports, Science and Technology of Japan (MEXT); by Grants-in-Aid for Scientific Research (B) (Grants 21300111 and 22300100) and for Challenging Exploratory Research (Grant 23651202) from JSPS; by the Grand Challenges in Next-Generation Integrated Simulation of Living Matter and the Computational Materials Science Initiative, a part of the Development and Use of the Next-Generation Supercomputer Project of MEXT; by the Platform for Drug Design, Informatics and Structural Life Sciences (MEXT); by the X-ray Free Electron Laser Priority Strategy Program (MEXT); and by the Elements Strategy Initiative for Catalysts & Batteries (MEXT).

■ REFERENCES

(1) Futai, M.; Kanazawa, H. Structure and Function of Proton-Translocating Adenosine Triphosphatase (F_0F_1): Biochemical and Molecular Biological Approaches. *Microbiol. Rev.* **1983**, *47*, 285−312.
(2) Futai, M.; Noumi, T.; Maeda, M. ATP Synthase (H^+-ATPase): Results by Combined Biochemical and Molecular Biological Approaches. *Annu. Rev. Biochem.* **1989**, *58*, 111−136.
(3) Senior, A. E. The Proton-Translocating ATPase of *Escherichia coli*. *Annu. Rev. Biophys. Biophys. Chem.* **1990**, *19*, 7−41.
(4) Pedersen, P. L.; Amzel, L. M. ATP Synthases. Structure, Reaction Center, Mechanism, and Regulation of One of Nature's Most Unique Machines. *J. Biol. Chem.* **1993**, *268*, 9937−9940.
(5) Boyer, P. D. The ATP Synthase—A Splendid Molecular Machine. *Annu. Rev. Biochem.* **1997**, *66*, 717−749.
(6) Walker, J. E. ATP Synthesis by Rotary Catalysis (Nobel Lecture). *Angew. Chem., Int. Ed.* **1998**, *37*, 2308−2319.
(7) Weber, J.; Senior, A. E. ATP Synthase: What We Know About ATP Hydrolysis and What We Do Not Know About ATP Synthesis. *Biochim. Biophys. Acta* **2000**, *1458*, 300−309.
(8) Kinosita, K., Jr.; Yasuda, R.; Noji, H.; Ishiwata, S.; Yoshida, M. F_1-ATPase: A Rotary Motor Made of a Single Molecule. *Cell* **1998**, *93*, 21−24.
(9) Gao, Y. Q.; Yang, W.; Karplus, M. A Structure-Based Model for the Synthesis and Hydrolysis of ATP by F_1-ATPase. *Cell* **2005**, *123*, 195−205.
(10) Karplus, M.; Gao, Y. Q. Biomolecular Motors: the F_1-ATPase Paradigm. *Curr. Opin. Struct. Biol.* **2004**, *14*, 250−259.
(11) Noji, H.; Yasuda, R.; Yoshida, M.; Kinosita, K., Jr. Direct Observation of the Rotation of F_1-ATPase. *Nature* **1997**, *386*, 299−302.
(12) Itoh, H.; Takahashi, A.; Adachi, K.; Noji, H.; Yasuda, R.; Yoshida, M.; Kinosita, K., Jr. Mechanically Driven ATP Synthesis by F_1-ATPase. *Nature* **2004**, *427*, 465−468.
(13) Rastogi, V. K.; Girvin, M. E. Structural Changes Linked to Proton Translocation by Subunit c of the ATP Synthase. *Nature* **1999**, *402*, 263−268.
(14) Abrahams, J. P.; Leslie, A. G.; Lutter, R.; Walker, J. E. Structure at 2.8 Å Resolution of F_1-ATPase from Bovine Heart Mitochondria. *Nature* **1994**, *370*, 621−628.
(15) Yasuda, R.; Noji, H.; Kinosita, K., Jr.; Yoshida, M. F_1-ATPase is a Highly Efficient Motor That Rotates with Discrete 120-degree Steps. *Cell* **1998**, *93*, 1117−1124.
(16) Yasuda, R.; Noji, H.; Yoshida, M.; Kinosita, K., Jr.; Itoh, H. Resolution of Distinct Rotational Substeps by Submillisecond Kinetic Analysis of F_1-ATPase. *Nature* **2001**, *410*, 898−904.
(17) Okuno, D.; Fujisawa, R.; Iino, R.; Hirono-Hara, Y.; Imamura, H.; Noji, H. Correlation Between the Conformational States of F_1-ATPase as Determined from Its Crystal Structure and Single-Molecule Rotation. *Proc. Natl. Acad. Sci. U.S.A.* **2008**, *105*, 20722−20727.
(18) Masaike, T.; Koyama-Horibe, F.; Oiwa, K.; Yoshida, M.; Nishizaka, T. Cooperative Three-Step Motions in Catalytic Subunits of F_1-ATPase Correlate with 80° and 40° Substep Rotations. *Nat. Struct. Mol. Biol.* **2008**, *15*, 1326−1333.
(19) Shimabukuro, K.; Yasuda, R.; Muneyuki, E.; Hara, K. Y.; Kinosita, K., Jr.; Yoshida, M. Catalysis and Rotation of F_1 Motor: Cleavage of ATP at the Catalytic Site Occurs in 1 ms Before 40° Substep Rotation. *Proc. Natl. Acad. Sci. U.S.A.* **2003**, *100*, 14731−14736.
(20) Adachi, K.; Oiwa, K.; Nishizaka, T.; Furuike, S.; Noji, H.; Itoh, H.; Yoshida, M.; Kinosita, K., Jr. Coupling of Rotation and Catalysis in F_1-ATPase Revealed by Single-Molecule Imaging and Manipulation. *Cell* **2007**, *130*, 309−321.
(21) Dittrich, M.; Hayashi, S.; Schulten, K. On the Mechanism of ATP Hydrolysis in F_1-ATPase. *Biophys. J.* **2003**, *85*, 2253−2266.

(22) Dittrich, M.; Hayashi, S.; Schulten, K. ATP hydrolysis in the β_{TP} and β_{DP} Catalytic Sites of F_1-ATPase. *Biophys. J.* **2004**, *87*, 2954−2967.
(23) Hayashi, S.; Ueno, H.; Shaikh, A. R.; Umemura, M.; Kamiya, M.; Ito, Y.; Ikeguchi, M.; Komoriya, Y.; Iino, R.; Noji, H. Molecular Mechanism of ATP Hydrolysis in F_1-ATPase Revealed by Molecular Simulations and Single-Molecule Observations. *J. Am. Chem. Soc.* **2012**, *134*, 8447−8454.
(24) Cui, Q.; Li, G.; Ma, J.; Karplus, M. A Normal Mode Analysis of Structural Plasticity in the Biomolecular Motor F_1-ATPase. *J. Mol. Biol.* **2004**, *340*, 345−372.
(25) Böckmann, R. A.; Grubmüller, H. Nanoseconds Molecular Dynamics Simulation of Primary Mechanical Energy Transfer Steps in F_1-ATP Synthase. *Nat. Struct. Biol.* **2002**, *9*, 198−202.
(26) Czub, J.; Grubmüller, H. Torsional Elasticity and Energetics of F_1-ATPase. *Proc. Natl. Acad. Sci. U.S.A.* **2011**, *108*, 7408−7413.
(27) Ma, J.; Flynn, T. C.; Cui, Q.; Leslie, A. G. W.; Walker, J. E.; Karplus, M. A Dynamic Analysis of the Rotation Mechanism for Conformational Change in F_1-ATPase. *Structure* **2002**, *10*, 921−931.
(28) Gao, Y. Q.; Yang, W.; Marcus, R. A.; Karplus, M. A Model for the Cooperative Free Energy Transduction and Kinetics of ATP Hydrolysis by F_1-ATPase. *Proc. Natl. Acad. Sci. U.S.A.* **2003**, *100*, 11239−11244.
(29) Pu, J.; Karplus, M. A Model for the Cooperative Free Energy Transduction and Kinetics of ATP Hydrolysis by F_1-ATPase. *Proc. Natl. Acad. Sci. U.S.A.* **2008**, *105*, 1192−1197.
(30) Antes, I.; Chandler, D.; Wang, H.; Oster, G. The Unbinding of ATP from F_1-ATPase. *Biophys. J.* **2003**, *85*, 695−706.
(31) Koga, N.; Takada, S. Folding-Based Molecular Simulations Reveal Mechanisms of the Rotary Motor F_1-ATPase. *Proc. Natl. Acad. Sci. U.S.A.* **2006**, *103*, 5367−5372.
(32) Kleinekathöfer, U.; Isralewitz, B.; Dittrich, M.; Schulten, K. Domain Motion of Individual F_1-ATPase β-Subunits during Unbiased Molecular Dynamics Simulations. *J. Phys. Chem. A* **2011**, *115*, 7267−7274.
(33) Ito, Y.; Ikeguchi, M. Structural Fluctuation and Concerted Motions in F_1-ATPase: A Molecular Dynamics Study. *J. Comput. Chem.* **2010**, *31*, 2175−2185.
(34) Ito, Y.; Oroguchi, T.; Ikeguchi, M. Mechanism of the Conformational Change of the F_1-ATPase β Subunit Revealed by Free Energy Simulations. *J. Am. Chem. Soc.* **2011**, *133*, 3372−3380.
(35) Yoshidome, T.; Ito, Y.; Ikeguchi, M.; Kinoshita, M. On the Rotation Mechanism of F_1-ATPase: Crucial Importance of Water-Entropy Effect. *J. Am. Chem. Soc.* **2011**, *133*, 4030−4039.
(36) Furuike, S.; Hossain, M. D.; Maki, Y.; Adachi, K.; Suzuki, T.; Kohori, A.; Itoh, H.; Yoshida, M.; Kinosita, K., Jr. Axle-Less F_1-ATPase Rotates in the Correct Direction. *Science* **2008**, *319*, 955−958.
(37) Hossain, M. D.; Furuike, S.; Maki, Y.; Adachi, K.; Suzuki, T.; Kohori, A.; Itoh, H.; Yoshida, M.; Kinosita, K., Jr. Neither Helix in the Coiled Coil Region of the Axle of F_1-ATPase Plays a Significant Role in Torque Production. *Biophys. J.* **2008**, *95*, 4837−4844.
(38) Uchihashi, T.; Iino, R.; Ando, T.; Noji, H. High-Speed Atomic Force Microscopy Reveals Rotary Catalysis of Rotorless. *Science* **2011**, *333*, 755−758.
(39) Kabaleeswaran, V.; Puri, N.; Walker, J. E.; Leslie, A. G. W.; Mueller, D. M. Novel Features of the Rotary Catalytic Mechanism Revealed in the Structure of Yeast F_1-ATPase. *EMBO J.* **2006**, *25*, 5433−5442.
(40) Watanabe, R.; Iino, R.; Noji, H. Phosphate-Release in F_1-ATPase Catalytic Cycle Follows ADP Release. *Nat. Chem. Biol.* **2010**, *6*, 814−820.
(41) Ikeguchi, M.; Ueno, J.; Sato, M.; Kidera, A. Protein Structural Change upon Ligand Binding: Linear Response Theory. *Phys. Rev. Lett.* **2005**, *94*, 078102.
(42) Ito, Y.; Ikeguchi, M. Molecular Dynamics Simulations of the Isolated β Subunit of F_1-ATPase. *Chem. Phys. Lett.* **2010**, *490*, 80−83.
(43) Sali, A.; Blundell, T. L. Comparative Protein Modelling by Satisfaction of Spatial Restraints. *J. Mol. Biol.* **1993**, *234*, 779−815.
(44) Gibbons, C.; Montgomery, M. G.; Leslie, A. G. W.; Walker, J. E. The Structure of the Central Stalk in Bovine F_1-ATPase at 2.4 Å Resolution. *Nat. Struct. Biol.* **2000**, *7*, 1055−1061.
(45) Ye, Y.; Godzik, A. Flexible Structure Alignment by Chaining Aligned Fragment Pairs Allowing Twists. *Bioinformatics* **2003**, *19* (Suppl 2), II246−II255.
(46) Ikeguchi, M. Partial Rigid-Body Dynamics in NPT, NPAT and NPγT Ensembles for Proteins and Membranes. *J. Comput. Chem.* **2004**, *25*, 529−541.
(47) MacKerell, A. D.; et al. All-Atom Empirical Potential for Molecular Modeling and Dynamics Studies of Proteins. *J. Phys. Chem. B* **1998**, *102*, 3586−3616.
(48) MacKerell, A. D., Jr.; Feig, M.; Brooks, C. L., III. Extending the Treatment of Backbone Energetics in Protein Force Fields: Limitations of Gas-Phase Quantum Mechanics in Reproducing Protein Conformational Distributions in Molecular Dynamics Simulations. *J. Comput. Chem.* **2004**, *25*, 1400−1415.
(49) Jorgensen, W. L.; Chandrasekhar, J.; Madura, J. D.; Impey, R. W.; Klein, M. L. Comparison of Simple Potential Functions for Simulating Liquid Water. *J. Chem. Phys.* **1983**, *79*, 926−935.
(50) Essmann, U.; Perera, L.; Berkowitz, M. L.; Darden, T.; Lee, H.; Pedersen, L. G. A Smooth Particle Mesh Ewald Method. *J. Chem. Phys.* **1995**, *103*, 8577−8593.
(51) Oroguchi, T.; Hashimoto, H.; Shimizu, T.; Sato, M.; Ikeguchi, M. Intrinsic Dynamics of Restriction Endonuclease EcoO109I Studied by Molecular Dynamics Simulations and X-Ray Scattering Data Analysis. *Biophys. J.* **2009**, *96*, 2808−2822.
(52) Yoshidome, T.; Ito, Y.; Matubayasi, N.; Ikeguchi, M.; Kinoshita, M. Structural Characteristics of Yeast F_1-ATPase before and after 16-degree Rotation of the γ Subunit: Theoretical Analysis Focused on the Water-Entropy Effect. *J. Chem. Phys.* **2012**, *137*, 035102.
(53) Kinoshita, M.; Iba, S.; Harada, M. Interaction between Macroparticles in Aqueous Electrolytes. *J. Chem. Phys.* **1996**, *105*, 2487−2499.
(54) Kinoshita, M.; Harano, Y. Potential of Mean Force between Solute Atoms in Salt Solution: Effects Due to Salt Species and Relevance to Conformational Transition of Biomolecules. *Bull. Chem. Soc. Jpn.* **2005**, *78*, 1431−1441.
(55) Okazaki, K.; Takada, S. Structural Comparison of F_1-ATPase: Interplay among Enzyme Structures, Catalysis, and Rotations. *Structure* **2011**, *19*, 588−598.
(56) Nishizaka, T.; Oiwa, K.; Noji, H.; Kimura, S.; Muneyuki, E.; Yoshida, M.; Kinosita, K., Jr. Chemomechanical Coupling in F_1-ATPase Revealed by Simultaneous Observation of Nucleotide Kinetics and Rotation. *Nat. Struct. Mol. Biol.* **2004**, *11*, 142−148.
(57) Watanabe, R.; Okuno, D.; Sakakihara, S.; Shimabukuro, K.; Iino, R.; Yoshida, M.; Noji, H. Mechanical Modulation of Catalytic Power on F_1-ATPase. *Nat. Chem. Biol.* **2012**, *8*, 86−92.